ARMA 14-7466

Near-surface principal stress trajectories in Alpine valleys (Grimsel region, Switzerland) as inferred from exfoliation fracture plumose structure axes and numerical modeling

Ziegler, M., Loew, S., Valley, B., and Amann, F.
ETH Zurich, Department of Earth Sciences, Zurich, Switzerland

This paper was prepared for presentation at the 48th US Rock Mechanics / Geomechanics Symposium held in Minneapolis, MN, USA, 1-4 June 2014.

ABSTRACT: In this study we will show how fractographic (i.e., fracture surface morphology) data of exfoliation fractures (i.e., fractures subparallel to landscape surfaces limited to near-surface rock masses) and three-dimensional numerical modeling can be used to infer orientations of principal rock mass stresses in topographically complex Alpine areas. Analysis of exfoliation fracture plumose axes, i.e., fractographic features that indicate main fracture propagation directions, and supposed local maximum compressive principal stress (σ_1) orientations at the time of fracture formation, suggests complex directional trends of near-surface σ_1 within trough valleys of the Grimsel region (central Swiss Alps). We investigated near-surface stress tensors with a three-dimensional, elastic numerical model to 1. deduce evidence that plumose axes form parallel to σ_1 in an overall compressive (far-field) stress field, and to 2. increase our knowledge of near-surface stress orientations in Alpine settings. Model results illustrate that superposition of topographic stresses with realistic horizontal strains reveals complex near-surface σ_1 trajectories that widely follow the patterns of plumose axes. The model results demonstrate large variations of stress orientations, which cannot be captured by small numbers of classical stress measurements. *In-situ* stress measurements support exfoliation fracture formation under compression and principal stress directions as inferred from our numerical model.

1. INTRODUCTION

Characterization of rock mass stresses is of great importance during design and construction phases of many geotechnical projects, such as surface mining (e.g., quarrying), underground excavations (e.g., tunnels and shafts), and for analyzing slope stability. However, rock stress data are commonly rare, and in many cases come from a very limited number of boreholes and borehole-based *in-situ* stress measurements. In early project phases there might even be no such stress data at all.

To date, most analytical and numerical studies on topographically-induced alteration of gravitational, tectonic, and exhumation-induced remnant stresses focused on two-dimensional cross valley geometries illustrating in-plane stress rotation (i.e., parallel to valley cross profile), occurrence of tensile and compressive stresses, and changes of principal stress magnitudes. These studies contributed substantially to our understanding of stresses in (alpine) valley slopes [1–5]. Though, model results were rarely compared with local *in-situ* or palaeostress data. In addition, the three-dimensional orientations of principal stresses remained poorly understood.

The granitic rock mass of the Grimsel region, located in the Central Alps of Switzerland between the town of Guttannen and Grimsel Pass, contains well-developed Pleistocene exfoliation joints[1] (i.e., joints that follow present or former landscape forms; also known as sheet or sheeting joints [6]) up to maximum depths of about 200 m below ground surface (bgs.) and within different landforms, such as trough valleys [7]. These joints are commonly decorated by fractographic markings (joint surface morphologies) like radial plumose structures that typically show a plumose axis (Fig. 1). Plumose axes propagate from a fracture origin in two opposing directions (i.e., they consist of two semi-axes) and mark the locations of fastest fracture propagation and greatest stress intensity during fracture growth [8]. Exfoliation joints are thought to form under high differential principal stresses ($\sigma_1 \geq \sigma_2 >> \sigma_3$; compressive stresses are positive) with compressive σ_1 and σ_2 oriented parallel to the fracture plane [6, 9]. *In-situ* stress measurement results and stress-induced rock mass failures in shallow subsurface galleries, such as spalling along tunnel walls,

[1] In this paper we use the term *exfoliation joint* when referring to a single, continuous surface. This surface may, however, be composed of several coplanar individual *exfoliation fractures* with distinct fracture origins.

support such high near-surface maximum and intermediate compressive stresses in the Grimsel region [10]. High near-surface compressive stresses can originate from: 1. the elastic response of laterally confined rock mass to erosional unloading [11–13], 2. ice unloading during deglaciation [14], 3. active regional tectonics [15–17], 4. topographic perturbation in areas of high relief topography [2, 18, 19], or 5. a combination of these mechanisms [1]. We assume that σ_1 lies parallel to the plumose axis at the time of fracture propagation. Thus, the orientations of plumose axes on exfoliation joints could be used as a proxy for near-surface palaeostress directions, and, in case of recent exfoliation fractures, contemporary stress directions (cf., [8]). This article supports this hypothesis by comparing fractographically-inferred stress directions with stress directions calculated utilizing a three-dimensional finite-difference stress model that incorporates the real topography of the Grimsel landscape. Furthermore, this paper aims to illustrate the complexity and patterns of near-surface stress orientations, which can be estimated from fractographic analyses and simplified numerical models.

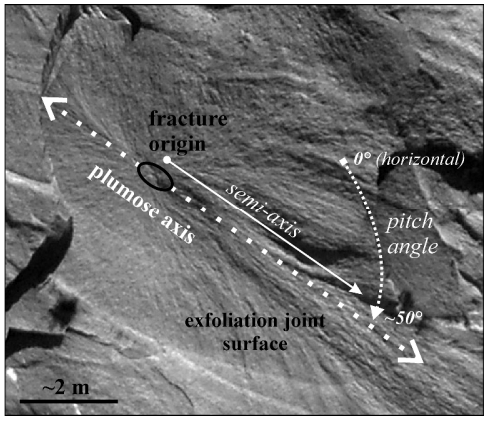

Fig. 1. Example of a radial plumose structure on a steep exfoliation joint northeast of Lake Räterichsboden (Fig. 3). Dotted arrows mark the plumose axis and major fracture propagation directions, respectively.

2. THE GRIMSEL STUDY SITE

2.1. *Geomorphological and lithological overview*

The Grimsel region is located in the upper Aar valley of the high Swiss Alps and ranges in elevation from about 1 to 3 km above sea level (asl.). Its morphology contains landforms of distinct ages (Pleistocene and pre-Pleistocene) and origin (glacial and fluvial) of which inner-trough valleys are most prominent [7]. Typical cross valley profiles contain (from crest to valley bottom): 1. glacial cirques or (sharp) kinks (i.e., glacial trimlines), 2. gently inclined, roughly linear upper valley slopes, 3. (convex) valley shoulders characterizing the boundary to 4. inner, steeper U-shaped trough valley, and 5. inner-valley gorge. Fig. 2 shows an elevation model of the area with a 25 m grid size (DHM25, swisstopo). The main inner-trough valley strikes about W-E to WSW-ENE west of Grimsel Pass and trends towards NNW north of Grimsel Pass.

Rock mass of the Grimsel region consists primarily of late Variscan intrusive rocks of the central Aar Massif (mainly Central Aar Granite and Grimsel Granodiorite; Fig. 2). These are surrounded by primarily older, polymetamorphic gneisses and schists, known as *Altkristallin* (Ger.) [20].

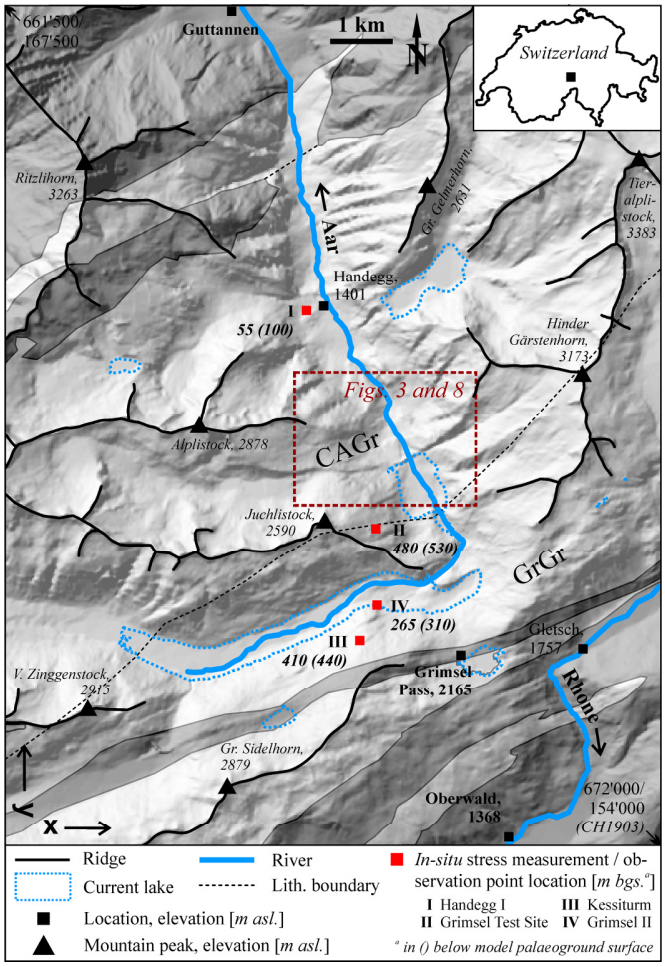

Fig. 2. Digital elevation model (DHM25) of the Grimsel area. Rock mass mainly consists of Carboniferous intrusives, such as Central Aar Granite (CAGr) and Grimsel Granodiorite (GrGr). Dark grey colored areas predominantly contain pre-Variscan gneisses, schists, and migmatites (Ziegler et al. [7], and references therein). The shown area corresponds to the modeled area (Fig. 5).

2.2. *In-situ stress measurements*

Stress measurement data of the Grimsel area come from the shallower and deeper subsurface (between about 40 and 680 m bgs.). In the course of preliminary projects for new subsurface hydropower constructions of Kraftwerke Oberhasli AG (KWO, Innertkirchen), borehole-based *in-situ* stress measurements utilizing hydraulic fracture method were conducted in 2009 (Handegg I) and 2011 (Kessiturm). Further data of the *in-situ* stress

state originate from overcoring and hydraulic fracture experiments at the NAGRA Grimsel Test Site (GTS; borehole GS 84.041 A). Additional overcoring data come from a niche located along an access gallery to the underground Grimsel II hydropower plant. Stress measurement locations and results are given in Fig. 2 and Table 1, respectively. The majority of stress measurements (in total 44) yield $S_H > S_h > S_v$ (see Fig. 9).

Table 1. Magnitude and orientation of *in-situ* stresses inferred from stress measurements in boreholes [21–24]

Location / overburden	S_v [MPa]	S_h [MPa]	S_H [MPa]	S_H orientation
Handegg I / 40–80 m	1.1–2.0	7.4–9.0	14.2–17.3	W-E (N86E ± 40)
Nagra GTS / 490–680 m	11–14	15–30	25–40	WNW-ESE to NNW-SSE
Grimsel II / 265 m	7.0	—	~20	N-S (N171E ± 11)
Kessiturm / 320–570 m	8.7–15.5	7.8–22.3	9.5–37.3	WNW-ESE

Vertical (S_v), minimum horizontal (S_h), and maximum horizontal (S_H) stress components.

3. ANALYSIS OF PLUMOSE STRUCTURES

3.1. Data acquisition and processing

The spatial coordinates (position, length, and direction) of a total of ~400 nearly straight (visible parts of) exfoliation fracture plumose semi-axes (for ease of reading referred to as the plumose axis) were surveyed with a reflectorless laser rangefinder (Vectronix VECTOR IV) connected to a mobile GPS station (Leica Zeno 15) with an integrated geographical information system (Leica Zeno GIS). The plumose axes are represented by three-dimensional polyline features consisting of up to eight linear segments with a mean of about three segments. Visible plumose axes lengths range from about 1.5 to 35.3 m with a median of 8.4 m. The mean trend and plunge of plumose axes (and fracture propagation directions) were calculated by linear best fit through the measured segments. Presentation of pitch angles, in contrast to cardinal directions, allows us to directly compare investigated exfoliation joint surfaces (and plumose structures) of variable orientation (data processing is described in more detail in [25]). The plumose axis pitch angle is the angle between a horizontal line and the (linearly approximated) plumose axis on the (inclined) fracture surface (Fig. 1). The exfoliation fracture (joint) orientation, necessary for calculating pitch angles, was estimated from LiDAR-based digital terrain models (open area minimum altimetric precision (1σ): ± 0.5 m) and/or from three-dimensional photogrammetric models. Plumose axis pitch angles contain information of the main direction(s) of plumose structure propagation relative to local slope topography. In this article we show representative data from plumose structures (~140 plumose axes) that originate from inner-trough valley slopes around Lake Räterichsboden, located in Central Aar Granite.

3.2. Plumose structures north of Lake Räterichsboden

Plumose structures around Lake Räterichsboden are situated within massive rock mass sections of Central Aar Granite (CAGr) (Figs. 2 and 3), and belong to exfoliation joints of Upper Pleistocene and Holocene age (denoted generation 3 and 4, according to Ziegler et al. [7]). We combine the data from generations 3 and 4 in this analysis based on common characteristics: 1. shallow occurrence (on the order of meters to few decameters below ground surface), 2. young ages (primarily fresh joint surfaces as compared to older exfoliation joint generations found in the region), and 3. orientations characteristically subparallel to today's ground surface. All plumose structures deviate from circularity and comprise a straight to slightly curved plumose axis. Complete plumose structures indicate that these axes form from a fracture origin in opposing directions and that exfoliation fractures propagated radially outwards (Fig. 1).

Fig. 3 presents an overview of the direction and length of plumose structures around Lake Räterichsboden. The calculated plumose axes pitch angles are presented in Fig. 4. These show that *left-* and *rightward* propagating axes dominate (68%). However, a considerable amount of plumose axes (32%) indicate *down-* and *upward* directed propagation (left, right, up, and down with respect to the line of sight from GPS stations; bin size 90°, i.e., four sectors of ± 45° from horizontal). Latter plumose axes occur, e.g., at location A close to the inner-trough valley bottom. Plotting pitch angles with a bin size of 2.5° shows local maxima at 20°, 35°, and 45°.

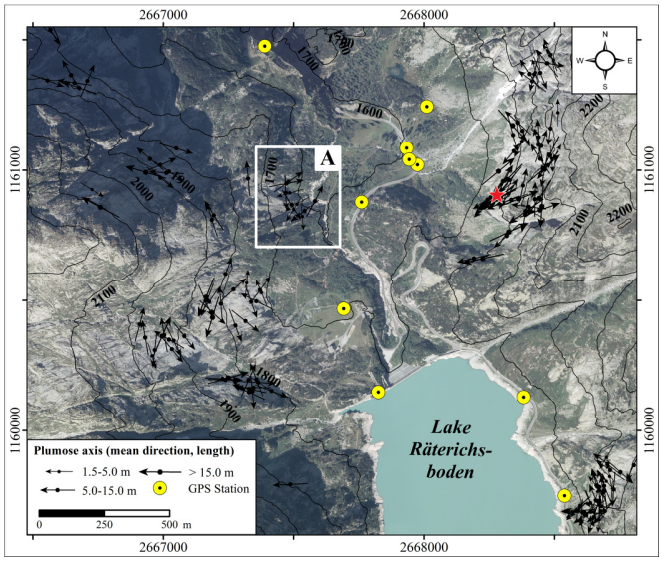

Fig. 3. Direction and length of plumose axes north and east of Lake Räterichsboden (for overview see Fig. 2; background: airborne orthophoto Swissimage, swisstopo). The red star marks the location of the plumose axis shown in Fig. 1.

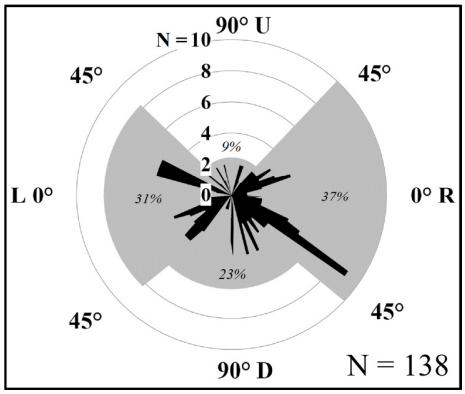

Fig. 4. Frequency (N) of exfoliation joint plumose axis pitch angles at the Lake Räterichsboden area. Pitch angle bin widths are 90° (grey sectors; L: left, R: right, D: down, U: up; N = 10 ≡ 37%) and 2.5° (black).

4. FINITE DIFFERENCE IN-SITU STRESS MODELING

4.1. Intact rock and rock mass properties

Based on (mean) values of intact granitic rock strength and elastic properties from Keusen et al. [26] we estimated mechanical rock mass properties (Table 2). We ignored lithological variations in the Grimsel area and used the rock properties of CAGr, the major rock type in the region, throughout the model. The rock mass consisting of CAGr is dissected by four widespread systematic joint sets with very wide mean joint spacing of ~15 m [27]. Thus, we only slightly reduced the mean Young's modulus of intact rock (E_i) to receive a continuum equivalent approximation of the Young's modulus of the rock mass (E_{rm}), accounting for joint compliance. Since the model is calibrated by increasing displacements at boundaries until target far-field stresses are reached within the model, the exact value of E_{rm} is of minor relevance.

Table 2. Material properties of (intact) granitic rock and rock mass (Central Aar Granite)

Parameter	Unit	Value
Density (ρ_i)	kg/m^3	2660 ± 23.8 (1σ)
Uniax. compr. strength (*UCS*)	MPa	169 ± 37.1 (1σ)
Young's modulus (E_i)	GPa	53.3 ± 11.0 (1σ)
Poisson's ratio (ν_i)	-	0.37 ± 0.12 (1σ)
Density (ρ_{rm})	kg/m^3	2660
Poisson's ratio (ν_{rm})	-	0.30
Young's modulus (E_{rm})	GPa	47
Gravitational acceleration (g)	m/s^2	9.81

1σ: range of the standard deviation.
i: intact rock; rm: rock mass.

4.2. Mesh setup

Our three-dimensional, rectangular 'block model' represents a height of z_m = 13.5 km (ranging from -10.0 to 3.5 km asl.), is 10.5 km wide (x_m is oriented W-E), and 13.5 km deep (y_m). We set a deep lower model boundary in order to reduce boundary effects from influencing near-surface stresses (e.g., [28]). To establish an approximately realistic recent topography, we modified the digital terrain model DHM25, presented in Fig. 2, by deleting artificial dams. The modified terrain model — ranging between about 1.0 km and 3.5 km asl. — was used to define the upper free boundary of the model. To avoid lateral boundary effects from influencing near-surface stresses in areas of primary interest, such as the area of Lake Räterichsboden, the model was located in a way that the target areas lie close to the center of the model. We discretized our model using ~8 million cubic elements that gradually decrease in size with increasing elevation from 500 m to ~15.5 m edge length (Fig. 5).

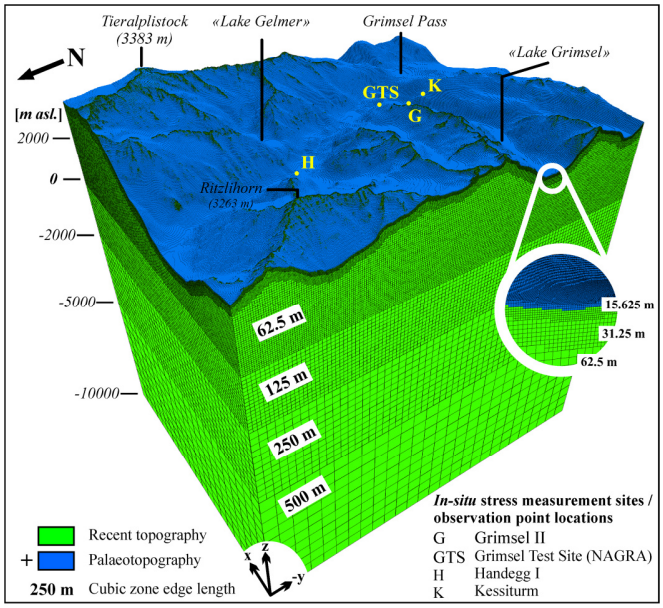

Fig. 5. Sketch of model discretization.

In order to avoid mesh effects influencing subsequent, near-surface stress tensor analysis, stress data was sampled along the recent topography in a 'palaeotopography model'. The 'sampling surface' is composed of approximately 0.6 Mio. elements (we thus only show a representative selection of modeled stress trajectories in Figs. 6–8). This palaeotopography model simulates a former erosional episode (~ early Upper Pleistocene) with palaeotopography roughly approximated by 'adding elevation' (i.e., rock mass) to the recent topography as a function of today's terrain altitude. The landscape elevation was gradually increased by 0 m at mountain peaks and up to ~45 m in valley bottoms, i.e., up to 3 elements of ~15 m edge length were added (Fig. 5).

We used three 'observation points' within the model for detailed investigation of principal stress magnitudes and orientations close to specific borehole intervals where *in-situ* stress measurements were conducted (Handegg I, GTS, and Kessiturm; Fig. 5). Each observation point is represented by a single model element.

4.3. *Boundary and initial gravitational stress conditions*

The today's (in situ) and palaeo stress states are the results of superposition of different stress sources. Within this study our aim was to investigate the effect of topographic perturbation on gravitational and horizontal compressive (tectonic, remnant) stresses within the uppermost parts of the Grimsel rock mass. We used a three-dimensional, finite difference model (FDM) utilizing FLAC3D 5.0 (Itasca, 2012).

First, we investigated loading by gravity until we reached equilibrium conditions ('gravitational stress model'). Our model is linearly elastic and rock mass properties were assumed to be isotropic. All external boundaries were established as 'rollers' to allow for boundary-parallel displacements, except the upper boundary (i.e., along topography), which we left unconstrained.

4.4. *Simulating high near-surface stresses*

We approximated additional horizontal (far-field) stress components from active tectonics and/or exhumation-induced (remnant) stresses, $S_{H,far\text{-}field}$ and $S_{h,far\text{-}field}$, by switching two adjacent, vertical external boundaries into displacement boundaries and stepwise compressing the model horizontally. Stress magnitudes and stress orientations were continuously tracked as the two boundaries were displaced simultaneously. This displacement aimed to simulate additional horizontal stress components as inferred from *in-situ* stress measurements at four locations within the study area (Table 1). We varied the boundary displacements in such a way as to create isotropic horizontal strains ($\varepsilon_{xx} = \varepsilon_{yy}$; 'isotropic strain model').

4.5. *Initial (gravitational) stress model results*

First, we simulated the influence of gravitational stresses to evaluate the effect of topographic perturbation on near-surface stresses. Minimum principal stresses (σ_3) are compressive at the landscape surface of higher elevation and in most parts of the subsurface. Tensile stresses develop primarily in the valley bottom of the ~N-S directed part of the Aar valley. Tensile stresses are limited to relatively shallow depth below the valley bottom (up to ~100 m below the model surface). Their orientations strike about perpendicular to the main valley axis and are subhorizontal in the valley bottom. In addition, the Grimsel Pass area and regions of comparably low elevation show tensile stresses. In contrast, the W-E to WSW-ENE directed main valley bottom west of Kessiturm does not exhibit tensile stresses. Compressive maximum principal stress (σ_1) orientations are slope-downward directed at the near-surface for most of the modeled area (Fig. 6).

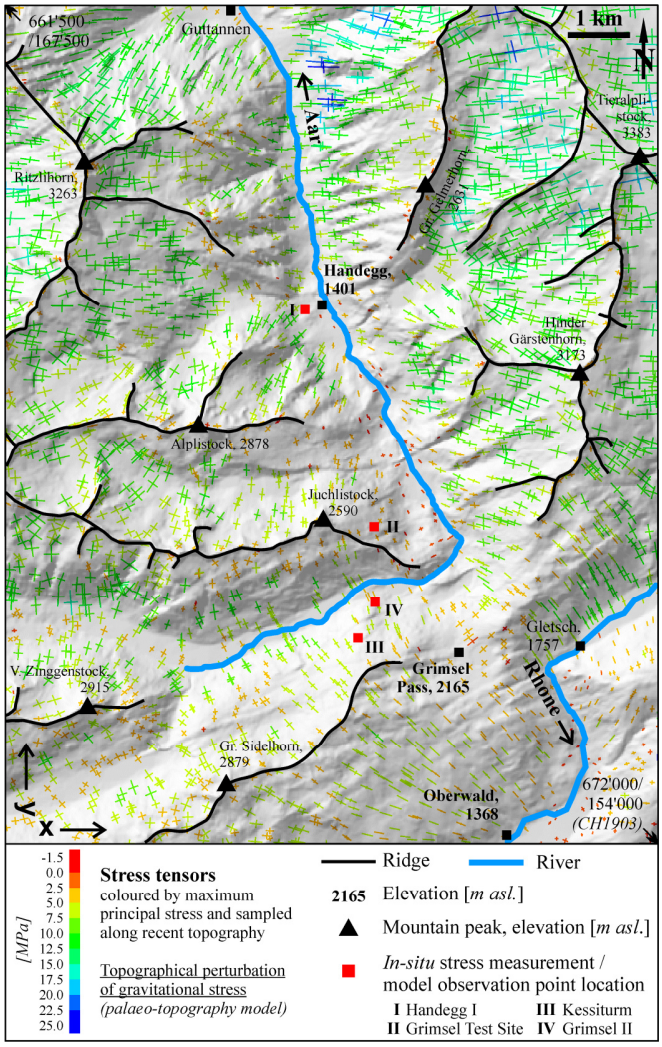

Fig. 6. Overview of projected stress tensor components σ_1 and σ_2 along the recent topography (± 15 m; palaeotopography model; topographic perturbation of gravitational stresses; background: modified DHM25). Owing to comparably small magnitudes the projections of σ_3 are too small to be recognized in Figs. 6–8.

4.6. *General results from isotropic strain model*

Besides unrealistic tensile stresses in valley bottoms and valley slopes (Table 1; cf., Section 5.1), the initial gravitational stress model results revealed that topographic perturbation of gravitational stresses alone cannot explain high compressive stress magnitudes derived from *in-situ* stress measurements (cf., Table 1 with Table 3). To roughly approximate active tectonic and/or remnant stress components from regional uplift and erosion, we stepwise applied horizontal displacements (note that in this article displacements are given in direction of the model y-axis) up to a maximum displacement of 10 m (~0.74 millistrain) at two adjacent vertical boundaries of our initial (gravitational stress) model. 10 m displacement along the y-axis equals an additional horizontal stress component ($S_{H,far\text{-}field} = S_{h,far\text{-}field}$) of ~49.6 MPa. Observing stress tensors close to the surface (up to ~45 m below the palaeotopography model surface) reveals

that principal stress orientations change little (< ~5°) after 3 m boundary displacements (~0.22 millistrain) within and close to valley bottoms and close to crest lines. In contrast, 'transition zones' located between lower and higher sections of inner-trough valley slopes and upper slopes above the valley shoulder (Section 2.1) show further, considerable stress rotations (>> 5°) above 3 m boundary displacement. In contrast to stress tensors located within the valley bottom and along mountain crests, stress tensors of these 'transition zones' are characterized by rather similar principal stress magnitudes, σ_1 and σ_2 (subparallel to the ground surface), and comparably prone to rotate under the given far-field stresses.

Table 3. Principal stresses at observation points in the gravitational stress model (recent topography)

Observation point (overburden [m])	σ_1 ($\cong S_v$) [MPa]	σ_2 ($\cong S_H$) [MPa]	σ_3 ($\cong S_h$) [MPa]
Handegg I (55)	3.6	2.6	1.0
GTS (480)	11.7	4.8	2.9
Kessiturm (410)	12.6	4.8	3.9

With increasing boundary displacement the initially steep plunges of σ_1 become flatter for the selected observation points in the model. Stress rotations considerably seize after about 4–8 m of horizontal boundary displacement (~0.30–0.59 millistrain), and maximum principal stress orientations at observation points finally plunge subhorizontally. Modeled and *in-situ* stress directions from Handegg I and Grimsel Test Site (GTS), closest to the Lake Räterichsboden area, show consistent results: about WNW-ESE to W-E oriented σ_1 at GTS from our model agrees well with WNW-ESE *in-situ* S_H ($\sim\sigma_1$) orientation inferred over most of the borehole length (cf., Table 1). Similarly, WSW-ENE to W-E σ_1 orientation at Handegg conforms to *in-situ* stress measurement results. Comparisons of modeled σ_1 with S_H magnitudes and orientations are rough estimations, since vertical and horizontal *in-situ* stresses may not coincide with principal stress orientations owing to, e.g., topographic stress perturbation.

The boundary displacements lead to approximately linear increases in the magnitudes of σ_1 and σ_2 at our observation points, while the magnitude of σ_3 remains relatively low. Changes in the ratios of σ_1 to σ_2 remain small (< ~5%) at boundary displacements greater than 3–5 m. Comparison of modeled principal stresses with *in-situ* stress results reveals that at observation point GTS a model boundary displacement of ~5 m (~0.37 millistrain) results in a stress state fairly similar to the measured *in-situ* stresses (the influence of palaeotopography with $\Delta S_v < 1.5$ *MPa* are negligible).

Assuming that exfoliation fractures start forming when σ_1 exceeds a crack initiation stress of 30–50% of the UCS (~50–85 MPa for mean UCS values of CAGr; Table 2) and the σ_1/σ_3-ratio is greater than ~10 (e.g., [29]), this stress state is reached within the valley bottom between Handegg and Lake Räterichsboden at approximately 4–8 m displacement (~0.29–0.59 millistrain). For subsequent analysis of stress tensors we use our 0.37 millistrain model (i.e., 5 m boundary displacement referring to additional horizontal stress of ~24.8 MPa).

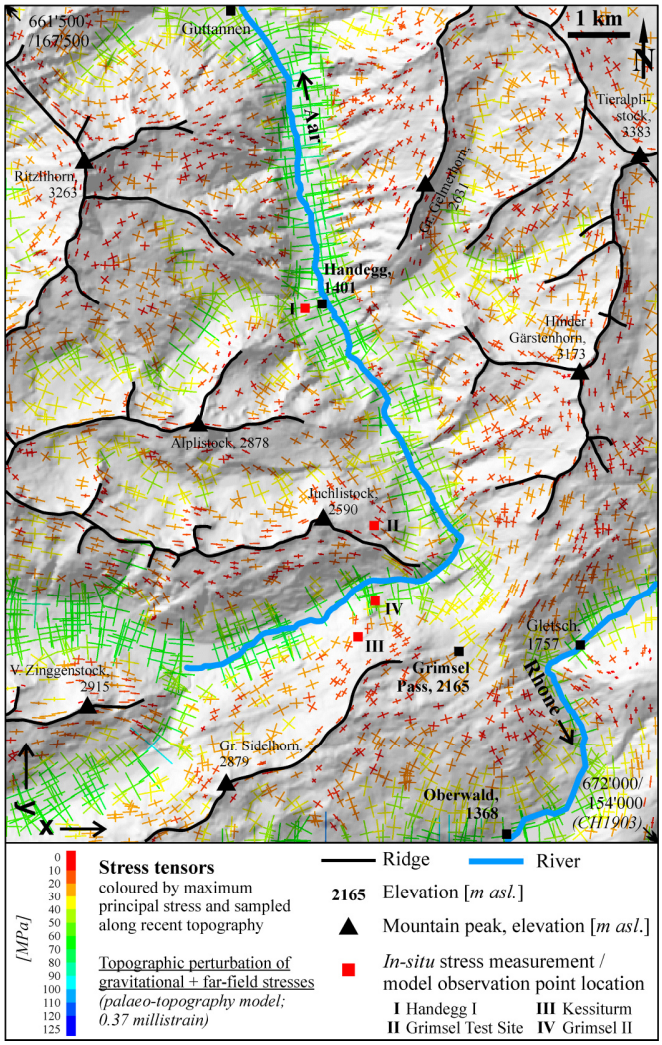

Fig. 7. Overview of projected stress tensor components σ_1 and σ_2 along the recent topography (± 15 m; palaeotopography model; topographic perturbation of gravitational and additional isotropic far-field stresses).

Fig. 7 presents an overview of stress tensors near the recent ground surface at 0.37 millistrain. The model results show concentration of compressive stresses with large σ_1/σ_3- and σ_2/σ_3-ratios at valley bottoms. Maximum principal stresses are oriented sub-perpendicular to valley axes within valley bottoms and lower ranges of inner-valley troughs in most of the modeled area. Higher slope sections, including mountain ridges, reveal subhorizontal to inclined orientations of σ_1. These are significant differences in comparison to the initial gravitational stress model.

4.7. *Comparison of fractographic and model results north of Lake Räterichsboden*

We now compare in detail modeled stress tensors, and in particular the directions of σ_1, with those assumed from plumose structure axes at the Lake Räterichsboden area (Section 3.2). In general, the numerically modeled and fractographically-inferred data sets reveal complex patterns of stress orientations that follow similar general trends. Fig. 8 shows stress trajectories at the Lake Räterichsboden area and illustrates that overall (km-scale) and local (on the order of few hundred meters) trends of σ_1 orientations derived from the two data sets are surprisingly consistent.

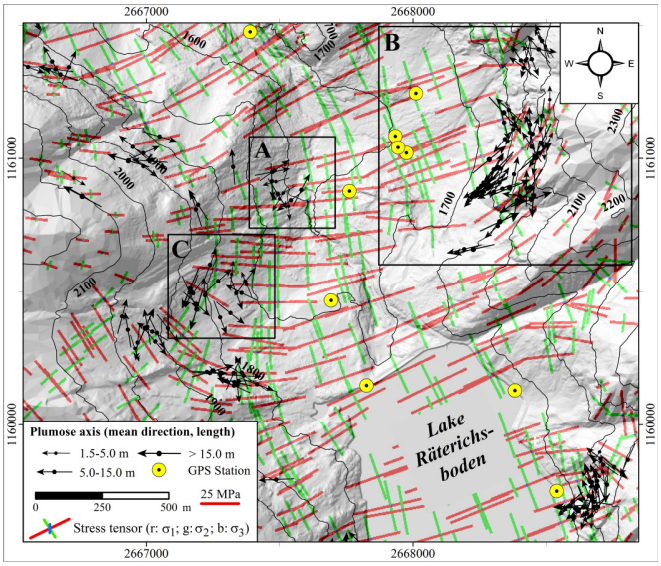

Fig. 8. Comparison of σ_1 directions inferred from plumose axes and modeled stress tensors (projected) around Lake Räterichsboden (0.37 millistrain model; topographic perturbation of gravitational and additional isotropic far-field stresses).

At the Aar valley bottom an about perpendicular strike, with respect to the valley axis, of σ_1 orientations inferred from plumose axes was captured by the model (e.g., at location A). Similarly, the model reflects subhorizontal to moderately inclined (pitch angle: 25–45°) σ_1 orientations at higher parts of trough valley slopes (e.g., at location B). Less consistent or contradictory stress orientations are evident, e.g., at location C. Mismatch between the two data sets seems to be most pronounced where modeled σ_1 and σ_2 are of similar magnitude.

5. DISCUSSION OF MODEL CONSTRAINTS AND NEAR-SURFACE PRINCIPAL STRESS ORIENTATIONS

5.1. *Observations from initial gravitational model*

Our numerical model with pure gravitational loading predicts tensile stresses in parts of main valley bottoms. This is consistent with results obtained from two-dimensional analytical and numerical models neglecting active tectonics or remnant stresses (e.g., [18, 28, 30]). However, subhorizontal tensile stresses in the valley bottom stand in contrast to stress measurement results from the Grimsel region.

5.2. *Strain magnitude and orientation*

Stepwise isotropic straining of the gravitational model showed that different locations, such as valley bottoms, steep inner-trough valley slopes, less steep upper valley slopes, and mountain crests react differently to additional horizontal strains. For detailed analysis of stress trajectories we used 0.37 millistrain, keeping most of the modeled area below or within a typical range of microcrack initiation close to the ground surface.

Model boundary displacements aimed to roughly simulate (active) tectonic strains and/or exhumation-induced stresses. Apart from topographic stress perturbation, compressive tectonics and exhumation are considered primary causes for high compressive, near-surface stresses with $k > 1$ (see references in Section 1; $k = S_{H/h}/S_v$). Fig. 9 illustrates the evolution of k with depth for our isotropic model, together with *in-situ* stress data from borehole measurements (k_{SH} and k_{Sh}). Despite local differences in *in-situ* k_{SH} (and k_{Sh}), the comparison reveals considerable overlaps between the *in-situ* and modeled stress states and further supports the strain magnitude used for stress tensor analysis.

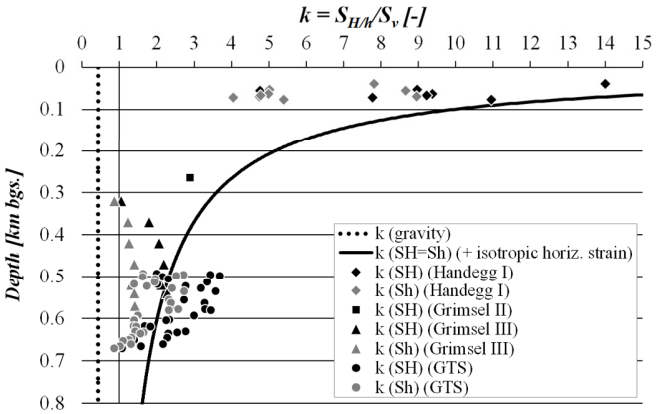

Fig. 9. Evolution of k with depth below ground (isotropic strain model; 0.37 millistrain; black curve), shown together with single, *in-situ* stress measurement results from four locations in the Grimsel area (Section 2.2). We calculated S_v using the load of the overburden, neglecting topographic effects.

Deepest stress measurements from the Kessiturm and GTS boreholes suggest anisotropic horizontal stresses with mean horizontal stress ratios S_H:S_h of ~1.5:1. In comparison, horizontal stress ratios at observation points GTS and Kessiturm are about 1.2 and 1.3, respectively. Thus, modeled horizontal stress ratios do not reach the *in-situ* horizontal stress ratios at the investigated locations. Anisotropic present-day strains (anisotropic far-field stresses) are supported by, e.g., inversion of regional GPS data [31], regional findings from earthquake

focal mechanisms, and stress measurements in boreholes (e.g., [32, 33]). The influence of anisotropic horizontal strains and strain directions on near-surface stresses will be investigated and presented in the future.

5.3. Near-surface principal stress orientations from isotropic strain model

As first approximation of rock mass stresses, active during exfoliation fracture formation, we analyzed a model simulating topographic perturbation of gravitational and additional isotropic far-field stresses. We revealed σ_1 trajectories that follow specific trends. Main and hanging trough valley bottoms comprise compressive stresses and σ_1 orientations about perpendicular to valley axes. This behaviour has been described previously by other researcher utilizing two-dimensional models of cross-valley profiles (e.g., [2]) and is to a certain extent analogue to well-studied compressive stress concentrations around boreholes and larger subsurface openings, such as tunnels (e.g., [34, 35]). S_H directions inferred from *in-situ* stress measurements at Handegg I and Grimsel II agree very well with and support modeled stress orientations within inner-trough valley bottoms. In addition, the majority of plumose structure axes located close to the valley bottom north of Lake Räterichsboden is aligned about perpendicular to the valley axis (Figs. 3 and 8: location A). At steeper slopes of inner-trough valleys, away from valley bottoms, σ_1 trajectories reduce in pitch angle, i.e., they rotate around the direction of σ_3 (oriented sub-perpendicular to the landscape surface). As a consequence, certain slope sections of inner-trough valleys contain locations where σ_1 and σ_2 are similar in magnitude (see 'transition zones' in Section 4.6). In our models these areas often locate below or nearby the valley shoulder, i.e., the transition from steep inner-valley to more gently inclined upper valley slopes. Our analysis of plumose structure axes supports such stress rotation. We yield good accordance at locations around Lake Räterichsboden (Fig. 8). These findings indicate that our palaeotopography isotropic strain model in combination with a mean stress tensor sampling depth of up to about 45 m below ground is capable of reproducing overall and local trends of stress trajectories during formation of generation 3 and 4 exfoliation joints.

6. CONCLUSIONS

Three-dimensional, elastic finite difference models illustrate that horizontal compressive strains, simulating active tectonic and/or exhumation-induced stresses, lead to changes in stress quality within valley bottoms of the Grimsel region, i.e., from unrealistic tensile to compressive stresses. While pure gravitational loading causes predominantly downslope oriented, compressive maximum principal stresses (σ_1) at slopes, superposition of gravitational and horizontal far-field stresses results in considerable stress rotation within slopes of alpine valleys. This rotation is characterized by a transition from downslope oriented σ_1 near inner-trough valley bottoms up to subhorizontally oriented σ_1 at higher slope sections up to mountain crests. Comparison of modeled, *in-situ* measured, and fractographically-inferred near-surface σ_1 ($\sim S_H$) orientations (i.e., using plumose axis data from Upper Pleistocene/Holocene exfoliation joints that are subparallel to today's landscape surface) unfolds consistent results. Thus, our numerical calculations strongly corroborate our hypothesis that exfoliation fracture plumose axes follow σ_1 trajectories, and suggest that directional trends of plumose axes can be used as proxy for σ_1 orientations. In addition, stress tensor analysis suggests that compressive stresses prevail within the uppermost parts of the modeled rock mass, proposing exfoliation fracture formation under overall far-field compressive principal stresses (i.e., $\sigma_1 \geq \sigma_2 > \sigma_3 > 0$).

Novel integration of *in-situ* stress data, fractographically-inferred stress orientations, and findings from simplified numerical modeling results in robust characterization of near-surface stress patterns within areas of complex topography, such as the Grimsel region of the Swiss Alps. Our numerical model demonstrates large variations of stress orientations, which cannot be captured by small numbers of classical stress measurements, and suggests to put more emphasis on interpreting *in-situ* stress data in the topographic and tectonic context.

7. ACKNOWLEDGEMENTS

This research is part of the Paraglacial Rock Slope Mechanics project supported by the Swiss National Science Foundation (SNF 135184). We thank Kraftwerke Oberhasli AG (Innertkirchen) for providing stress measurement data. Marc Hugentobler (ETH) substantially helped us with collecting fractographic data in the field.

8. REFERENCES

1. Savage, W.Z. and H.S. Swolfs. 1986. Tectonic and gravitational stress in long symmetric ridges and valleys. *JGR* 91: 3677–3685.
2. Miller, D.J. and T. Dunne. 1996. Topographic perturbations of regional stresses and consequent bedrock fracturing. *JGR* 101: 25,523–25,536.
3. Hasebe, N. and X. Wang. 2003. Irregular elastic half-plane gravity problem. *Int. J. Rock Mech. Min. Sci. & Geomech. Abstr.* 40: 863–875.
4. Kinakin, D. and D. Stead. 2005. Analysis of the distributions of stress in natural ridge forms: implications for the deformation mechanisms of rock slopes and the formation of sackung. *Geomorphology* 65: 85–100.
5. Leith, K.J. 2012. *Stress development and geomechanical controls on the geomorphic evolution of alpine valleys*. Ph.D. thesis. ETH Zurich (Switzerland).

6. Dale, T.N. 1923. *The commercial granites of New England.* Washington: Government Printing Office.

7. Ziegler, M., S. Loew, and J.R. Moore. 2013. Distribution and inferred age of exfoliation joints in the Aar Granite of the central Swiss Alps and relationship to Quaternary landscape evolution. *Geomorphology*: 344–362.

8. Kulander, B.R. and S.L. Dean. 1985. Hackle plume geometry and joint propagation dynamics. In: *Fundamentals of rock joints*, ed. O. Stephansson, 85–94. Luleå: Centek.

9. Martel, S.J. 2011. Mechanics of curved surfaces, with application to surface-parallel cracks. *Geophys. Res. Let.* 38: 1–6.

10. Ziegler, M. 2014. Age and formation mechanisms of exfoliation joints in the Aar Granites of the Central Alps (Grimsel region, Switzerland). Ph.D. thesis. ETH Zurich (Switzerland).

11. Voight, B. 1966. Beziehung zwischen grossen horizontalen Spannungen im Gebirge und der Tektonik und der Abtragung. In: *Proceedings of the First Congress of the International Society of Rock Mechanics*, ISRM, 51–56. Lisbon: Laboratorio Nacional de Engenharia Civil.

12. Nichols, T.C. 1980. Rebound, its nature and effect on engineering works. *Q. J. Eng. Geol. London* 13: 133–152.

13. Nadan, B.J. and T. Engelder. 2009. Microcracks in New England granitoids: A record of thermoelastic relaxation during exhumation of intracontinental crust. *Geological Society of America Bulletin* 121: 80–99.

14. Carlsson, A. and T. Olsson. 1982. High rock stresses as a consequence of glaciation. *Nature* 298: 739–742.

15. Park, R.G. 1988. *Geological structures and moving plates*. Glasgow (UK): Blackie and Sons.

16. Stephansson, O., C. Ljunggren, and L. Jing. 1991. Stress measurements and tectonic implications for Fennoscandia. *Tectonophysics* 189: 317–322.

17. Pascal, C., D. Roberts, and R.H. Gabrielsen. 2010. Tectonic significance of present-day stress relief phenomena in formerly glaciated regions. *J. Geol. Soc.* 167: 363–371.

18. Savage, W.Z., H.S. Swolfs, and P.S. Powers. 1985. Gravitational stresses in long symmetric ridges and valleys. *Int. J. Rock Mech. Min. Sci. & Geomech. Abstr.* 22: 291–302.

19. Molnar, P. 2004. Interactions among topographically induced elastic stress, static fatigue, and valley incision. *JGR* 109: 1–9.

20. Abrecht, J. 1994. Geologic units of the Aar massif and their pre-Alpine rock associations: a critical review: Kleinere Mitteilungen Nr. 95. Präalpine Entwicklung des Aar- und Gotthardmassivs. *Schweiz. Mineral. Petrogr. Mitt.* 74: 5–27.

21. Rummel, F. and G. Klee. 2009. *Durchführung von Hydraulik- und Hydrofrac-Spannungsmessungen in der Bohrung Handegg-1*. Mönchaltorf: Solexperts AG (internal report).

22. Pahl, A., S. Heusermann, V. Bräuer, and W. Glöggler. 1989. *Grimsel Test Site: Rock stress investigations.* NTB 88-39E. Baden: NAGRA.

23. Gruner, U. and H.-J. Ziegler. 2011. *Pumpspeicherwerk Grimsel 3. Sondierbohrung Kessiturm.* Bern: Kellerhals & Haefeli AG (internal report).

24. Illies, J.H. and G. Greiner. 1976. Regionales stress-Feld und Neotektonik in Mitteleuropa. *Oberrhein. geol. Abh.* 25: 1–40.

25. Ziegler, M., S. Loew and D. Bahat. (under revision). Exfoliation fracture mechanisms and near-surface stress orientations inferred from fractographic markings observed in the upper Aar valley (Swiss Alps). *Tectonophysics*.

26. Keusen, H.R., J. Ganguin, P. Schuler, and M. Buletti. 1989. *Grimsel test site.* NTB 87-14E. Baden: NAGRA.

27. Ferrari, F. 2014. *Rock mass characterization and spatial estimation of geomechanical properties through geostatistical techniques.* Ph.D. thesis. Universita degli studi di Milano (Italy).

28. Pan, E., B. Amadei, and W.Z. Savage. 1994. Gravitational stresses in long symmetric ridges and valleys in anisotropic rock. *Int. J. Rock Mech. Min. Sci. & Geomech. Abstr.* 31: 293–312.

29. Leith, K., F. Amann, J.R. Moore, A. Kos, and S. Loew. 2010. Conceptual modelling of near-surface extensional fracture in the Matter and Saas Valley, Switzerland. In: *Geologically Active, Proc. IAEG Congress, Auckland,* eds. Williams et al., 363–371.

30. Martel, S.J. and J.R. Muller. 2000. A two-dimensional boundary element method for calculating elastic gravitational stresses in slopes. *Pageoph* 157: 989–1007.

31. Tesauro, M., C. Hollenstein, R. Egli, A. Geiger, and H.-G. Kahle. 2006. Analysis of central western Europe deformation using GPS and seismic data. *J. Geodyn.* 42: 194–209.

32. Müller, B., M.L. Zoback, K. Fuchs, L. Mastin, S. Gregersen, and N. Pavoni. 1992. Regional patterns of tectonic stress in Europe. *JGR* 97: 11,783–11,803.

33. Sue, C., B. Delacou, J.-D. Champagnac, C. Allanic, P. Tricart, and M. Burkhard. 2007. Extensional neotectonics around the bend of the Western/Central Alps: an overview. *Int. J. Earth Sci.* 96: 1101–1129.

34. Bell, J.S. and D.I. Gough. 1979. Northeast-southwest compressive stress in Alberta: Evidence from oil wells. *Earth Planet. Sci. Let.* 45: 475–482.

35. Martin, C.D., P.K. Kaiser, and D.R. McCreath. 1999. Hoek-Brown parameters for predicting the depth of brittle failure around tunnels. *Can. Geotech. J.* 36: 136–151.